

Article

Nickel Oxide Nanoparticles on KIT-6: An Efficient Catalyst in Methane Combustion

Xiuhui Huang ^{1,*}, Wenkai Yang ¹, Zeqiu Li ¹, Qin Lou ¹, Ying Tian ²  and Junfeng Li ^{3,*}

¹ School of Energy and Power Engineering, University of Shanghai for Science and Technology, Shanghai 200093, China; 223370198@st.usst.edu.cn (W.Y.); lizeqiu@usst.edu.cn (Z.L.); louqin560916@163.com (Q.L.)

² School of Optical Electrical and Computer Engineering, University of Shanghai for Science and Technology, Shanghai 200093, China; tianying009@sina.com

³ Shanghai MCC20 Construction Co., Ltd., Shanghai 201999, China

* Correspondence: hxh@usst.edu.cn (X.H.); ljf@sh20mcc.cn (J.L.)

Abstract: KIT-6 silica with well-ordered three-dimensional (3D) mesopores has been synthesized as a support for nickel-based catalysts. Transmission Electron Microscopy (TEM) and low-angle X-ray Diffraction (XRD) analysis are used to ensure that the ordered 3D mesostructure is stable after NiO incorporation. In this study, the catalytic activities of the NiO/KIT-6 samples are investigated. Additionally, the results show that a 10 wt% NiO/KIT-6 catalyst exhibits high catalytic performance in methane combustion, with T_{10} , T_{50} and T_{90} being only 386 °C, 456 °C and 507 °C, respectively. Hydrogen Temperature Programmed Reduction (H_2 -TPR) studies have shown that the interaction between NiO and KIT-6 in the 10 wt% NiO/KIT-6 catalyst is weak. Methane Temperature programmed Surface Reaction (CH_4 -TPSR) results show that the surface oxygen of the NiO/KIT-6 catalyst allows it to exhibit a high catalytic performance. NiO/KIT-6 catalysts exhibit superior activities to SBA-15, MCF and SiO_2 support catalysts because KIT-6 has a higher surface area and ordered 3D mesopore connectivity, which is favorable for better NiO dispersion and peculiar diffusion for reactant and products. Furthermore, the used catalyst maintained an ordered mesostructure and reduction property.



Citation: Huang, X.; Yang, W.; Li, Z.; Lou, Q.; Tian, Y.; Li, J. Nickel Oxide Nanoparticles on KIT-6: An Efficient Catalyst in Methane Combustion. *Processes* **2023**, *11*, 1004. <https://doi.org/10.3390/pr11041004>

Academic Editors: Alina Pyka-Pajak, Francesca Raganati, Barbara Dolińska and Federica Raganati

Received: 21 February 2023

Revised: 16 March 2023

Accepted: 22 March 2023

Published: 26 March 2023



Copyright: © 2023 by the authors. Licensee MDPI, Basel, Switzerland. This article is an open access article distributed under the terms and conditions of the Creative Commons Attribution (CC BY) license (<https://creativecommons.org/licenses/by/4.0/>).

Keywords: nickel-based catalyst; KIT-6; methane combustion; high catalytic activity; 3D mesopore

1. Introduction

Methane is widely available, obtained from natural gas, coal mines and biogas. It is recognized as a cleaner hydrogen-rich energy compared to others because of its high hydrogen-to-carbon ratio and high calorific value. When methane is utilized, it can be directly discharged into the atmosphere, wasting resources and causing environmental pollution, and it has a low utilization efficiency and releases polluting gases when directly burned [1,2]. In recent years, the catalytic combustion of methane has increasingly captured the interest of researchers and industry professionals, as it offers notable advantages, such as high efficiency, safety and minimal emissions of pollutants, such as NO_x and CO [3,4]. The synthesis of catalysts with high activity, high resistance to sulfur poisoning, and high hydrothermal stability is crucial to the research on the catalytic combustion of methane, as methane is one of the most inert hydrocarbons. It has been found that noble metal-based catalysts (Pt, Pd, Rh, etc.) [5,6], especially supported palladium catalysts, show excellent activity during methane combustion. However, their development and industrial application are limited due to their high cost and rapid deactivation at high temperatures, as well as the fact they can cause poisoning. Non-noble metal-based catalysts, including perovskite-type catalysts, hexa-aluminate catalysts and transition metal oxide catalysts, etc., have garnered significant interest owing to their low price and high thermal stability,

but their poor low-temperature activity limited their development [7–9]. Transition metal-based catalysts have been widely investigated in methane combustion because of their good stability and low price [10,11]. As an efficient transition metal-based catalyst, there are some reports on the use of nickel-based catalysts in the combustion of methane. R.M. [12] studied the performance of an NiO/SiO₂ foam catalyst in the methane reforming reaction, which showed good stability and activity, mainly due to its good porosity and pore structure. Notably, at a reaction temperature of 600 °C, the methane conversion rate reached 42%. Huang [13] found that the catalytic performance of NiO/CeO₂ was significantly enhanced in CH₄ combustion, particularly when the NiO loading reached 10 wt%, and Chai R [14] found that the NiO/CeO₂ catalyst also showed high stability and good water resistance in CH₄ combustion. Likewise, A.S. Al-Fatesh [15] investigated the impact of an SiO₂ support on catalyst performance and discovered that as the amount of silica decreased, the catalyst demonstrated an improved CH₄ conversion rate and stability in methane catalytic decomposition. Lu Y [16] found that a suitable support was crucial in creating a highly effective nickel-based catalyst. In comparison to the Ni/MgO (111) catalyst, the Ce/Zr co-doped catalyst exhibited superior catalytic activity and stability. Differently, A.S. Al-Fatesh [17] investigated the effects of three different preparation methods on catalytic activity. It was found that the impregnation method can produce enough active sites on the catalyst surface to exhibit higher activity. Additionally, the addition of nickel can increase the methane conversion rate and H₂ yield up to 10%. Besides the above, factors such as the calcination temperature and catalyst surface area also affect the performance of the catalyst. Anis Hamza Fakeeha [18] investigated the effect of combustion temperature on the activity and stability of catalysts. Through experiments, it was found that Co/Al₂O₃-ZrO₂ catalysts exhibit metal-support interactions when calcined at temperatures ranging from 550 °C to 800 °C, which helps them resist sintering. At higher temperatures (800 °C), Ni/Co is uniformly distributed on the support, leading to improved coking resistance. In general, elevating the calcination temperature proves to be advantageous for enhancing catalyst performance. Anis Fakeeha [19] found that the Ni-Al-H-600 catalyst had the highest methane conversion rate and hydrogen production at 650 °C due to its larger surface area and pore volume, reaching 90% and 72%, respectively. Moreover, after being subjected to a reaction for seven hours at this temperature, it exhibited the highest activity and stability.

In other studies of the effect of nickel-based catalyst with different catalyst supports, mesoporous silica (such as MCM-41, SBA-15, KIT-6, MCF, etc.) has been widely used as a catalyst support because of its specific pore structure, high surface area, and thermal stability, and its ability to improve catalyst activity [20,21], especially SBA-15, which has ordered two-dimensional (2D) hexagonal channels and showed good catalytic effect in several reactions [22,23]. For example, Miao et al. [22] found that nickel-based SBA-15 catalysts have good catalytic stability and there is a stronger interaction between the nickel and support, as shown in the results of the CO methanation reaction. SBA-15 is also used as an effective support in methane combustion. For example, Murthy [24] and others improved the stability of the catalyst by fixing Pd on SBA-15 and uniformly dispersing it on the channel; this porous structure can inhibit Pd flow to prevent sintering. Additionally, the catalyst shows good thermal stability and catalytic activity in methane combustion.

KIT-6 has ordered 3D mesoporous channels, which makes it superior to catalysts with low-order channels (SBA-15) in mass transfer characteristics. Based on this advantage, KIT-6-based catalysts are superior to SBA-15-based catalysts in terms of reactant and product transport and catalyst activity [25]. In the research on KIT-6 in CO methanation, Lv Y [21] found that catalysts with high Ni contents showed good activity in CO methanation, owing to the unique 3D structure and large surface area of KIT-6. Congming Tang [26] characterized Ni/KIT-6 catalysts with different compositions using XRD and BET. The results indicated that the surface area and crystallinity of metal Ni in the catalysts were influenced by the reduction temperature. The prepared catalysts demonstrated impressive CH₄ and CO₂ conversion rates of 69.0% and 39.4%, respectively, while also exhibiting good stability. Rita Mahfouz [27] investigated the effect of Ce addition on the mesoporous

structure. Through characterization, it was found that Ce promotion led to significant destruction of the porous structure, while catalysts without promotion exhibited better catalytic performances.

The above research shows that most researchers focus on the study of KIT-6 in related fields, such as CO methanation and methane dry reforming. However, there is little research on the use of KIT-6 catalysts in methane catalytic combustion. Therefore, this article examines the characteristics of catalysts from the perspective of methane catalytic combustion to provide a reference and guidance for future research.

Herein, we have synthesized a series of mesoporous silica KIT-6 support NiO samples, which have ordered mesoporous structures similar to pure KIT-6 and NiO nanoparticles embedded into the pore channels. It was found that these NiO/KIT-6 catalysts have high activities for methane combustion due to their high surface area and distinctive structure.

2. Materials and Methods

2.1. Synthesis

KIT-6 was prepared as described previously [28]. In typical synthesis, 6 g of P123 is dissolved in 217 g of distilled water and 11.8 g of concentrated HCl (37 wt%), followed by the addition of 6 g of 1-butanol and continuous stirring at 35 °C after stirring for 1 h. Then, 12.9 g of TEOS is slowly added at 35 °C and stirring is carried out at 35 °C for 24 h. After this, the solution in its final form is moved into Teflon bottles and is maintained at 100 °C for 24 h. After hydrothermal treatment, filtering, washing with deionized water until neutral, and drying at room temperature are carried out. Then, the solution is calcined for 5 h under flowing air at 550 °C to remove the organic template.

The NiO/KIT-6 sample was prepared from Ni(NO₃)₂ aqueous solution via the impregnation approach. The NiO content varies between 1 wt% and 15 wt%. All samples were dried at 100 °C and then calcined for 4 h in air at 450 °C to acquire the final products.

For comparison, SBA-15, MCF and SiO₂ were synthesized and used as the supports, following a previous report [28–31]. Then, 10 wt% NiO/SBA-15, 10 wt% NiO/MCF and 10 wt% NiO/SiO₂ samples were prepared via an impregnation approach and using 10 wt% NiO/KIT-6.

2.2. Characterization

The XRD pattern was recorded on a Bruker D8 Focus diffractometer with a wavelength of 1.541 Å (40 kV, 40 mA, scanning step = 0.02°). The N₂ adsorption–desorption isotherms were measured at –196 °C using the Surface Area as well as Pore Size Analyzer of NOVA 4200e. Prior to measurement, the samples were outgassed for 4 h under vacuum at 180 °C. The BET surface area of samples was calculated using Brunauer–Emmett–Teller approach. The pore size distribution was calculated using the Barrett–Joyner–Halanda approach. The overall pore volume (V_p) was estimated to be 0.985 (P/P₀). The Fourier Transform Infrared (FT-IR) absorption spectrum was documented on the Nicolet NEXUS 670 FT-IR spectrometer, with thirty-two scans at 4 cm^{–1} effective resolution. After grinding the sample with KBr, the sample was analyzed on a thin wafer. H₂-TPR was used in the TCD detector. The sample (50 mg) is placed in a quartz tube reactor. Using 5 vol% H₂/N₂ mixture gas of 40 mL·min^{–1}, heated at room temperature to 800 °C at 10 °C·min^{–1}. The CH₄-TPSR reaction was carried out in quartz micro-reactor. A total of 200 mg of catalysts was pretreated in 500 °C for 30 min in 50 mL·min^{–1} 20 vol% O₂/He mixture gas. Following cooling, the sample at room temperature, 50 mL·min^{–1} 1 vol% CH₄/He were heated from room temperature to 800 °C at 10 °C·min^{–1}. A quadrupole mass spectrometer (INFICON Transpector 2) was used to analyze the exit gas. At *m/z* = 15, 18, 28, 32 and 44, the signals of CH₄, H₂O, CO, O₂, CO₂ were recorded, respectively.

2.3. Tests of Catalytic Activity

In this study, several kinds of NiO/KIT-6 catalysts in methane combustion were investigated in quartz tube reactor (Ø 6 mm) at atmospheric pressure. Reagent gas mixture

containing 1.0 vol% CH₄ + 4.0 vol% O₂ in Ar under the flow rate of 50 mL·min⁻¹ entered a catalyst (200 mg, 20–40 mesh) bed, resulting in a weight hourly space velocity (WHSV) of 15,000 mL·g⁻¹·h⁻¹. Online analysis of reactants and products was carried out using a TCD gas chromatograph (GC). The activities of catalyst were measured at a programmed temperature of 200 °C to 700 °C when heated at a rate of 5 °C·min⁻¹. T₁₀, T₅₀ and T₉₀ represent 10%, 50% and 90%, respectively, of the catalyst activity. Additionally, the experimental setup of the reactor used is shown in Figure 1.

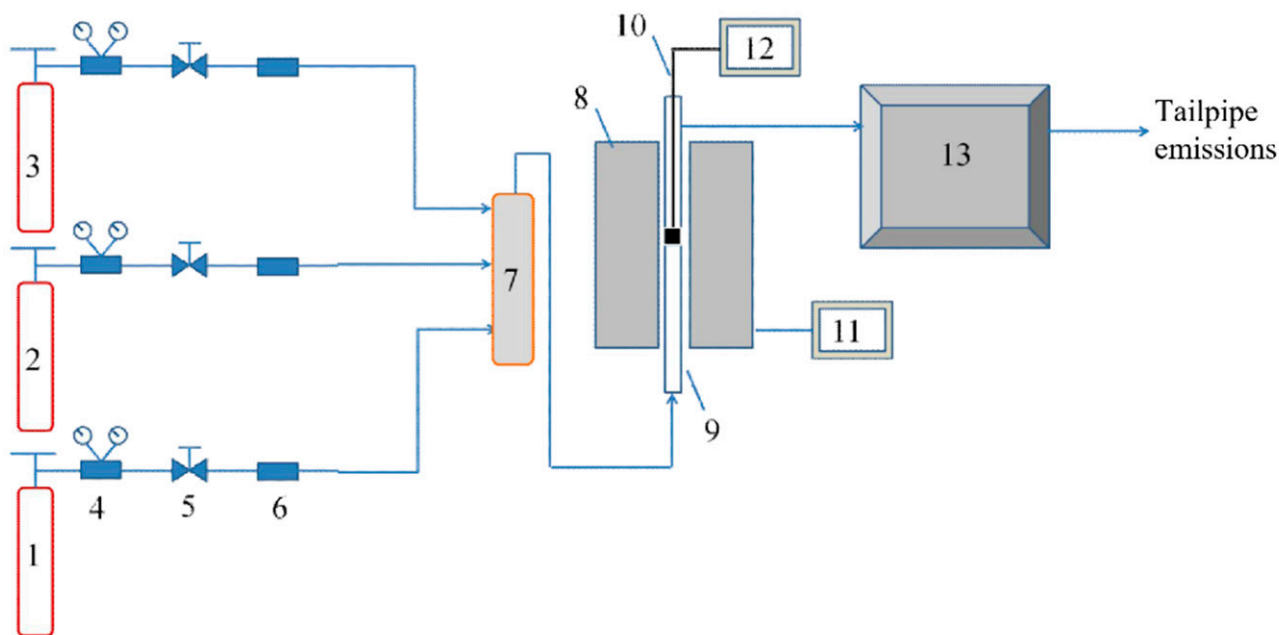


Figure 1. Catalyst methane catalytic combustion activity evaluation device diagram. 1. Ar; 2. O₂; 3. CH₄/CO; 4. Reduction Valve; 5. Stop Valve; 6. Mass Flowmeter; 7. Gas Mixing Tank; 8. Tube Heating Furnace; 9. Quartz Reactor; 10. Thermocouple; 11. Temperature Controller; 12. Digital Indicator; 13. Gas Chromatograph.

3. Results and Discussion

Figure 2a indicates XRD patterns at low angles for various NiO/KIT-6 catalysts. The XRD pattern of 1% NiO/KIT-6 identifies a sharp peak of intense intensity at $2\theta = 1.04$ as well as a hump in (220) planes, very similar to pure KIT-6 [28], indicating that the main well-ordered mesopore remains after NiO loading. The diffraction peak of (220) plane becomes weaker with increasing loading amount of NiO, which reveals that some mesoporous structures are destroyed when a mass of NiO nanoparticles are incorporated into the pore tunnel. Figure 2b shows wide-angle XRD patterns for NiO/KIT-6 catalysts. All the samples indicate diffraction peaks of NiO in the cubic phase (JCPDS file No. 65-2901). Moreover, NiO has a wide diffraction peak, indicating that NiO particles are highly dispersed on KIT-6. With the increase in loading amounts, NiO nanoparticles began to aggregate and NiO in the cubic phase exhibits sharp diffraction peaks.

In Figure 3, the TEM images of KIT-6 and 10% NiO/KIT-6 are shown. As shown in Figure 3a, for KIT-6 a well-ordered cubic array of mesopores was observed, with a pore size of approximately 8 nm. After supporting NiO, the cubic 3D uniform channel array of mesopores can still be seen clearly. The NiO particles were assembled in mesoporous channels, which showed irregular shapes, which was suitable for the porous structure of supports.

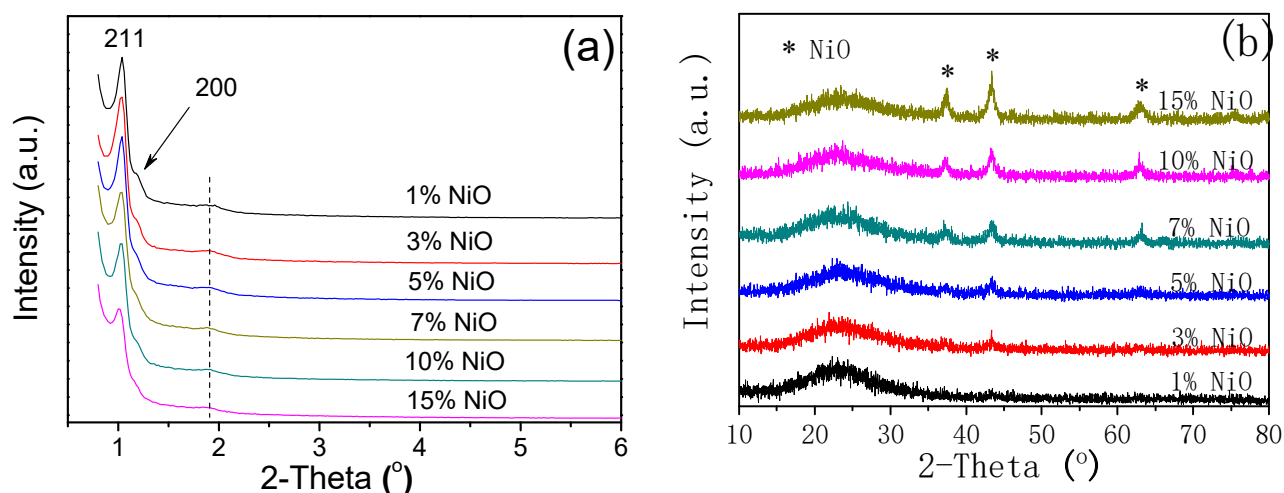


Figure 2. (a) Low-angle XRD patterns and (b) Wide-angle XRD patterns of NiO/KIT-6 catalysts with various NiO loading amounts (*NiO: NiO diffraction peak).

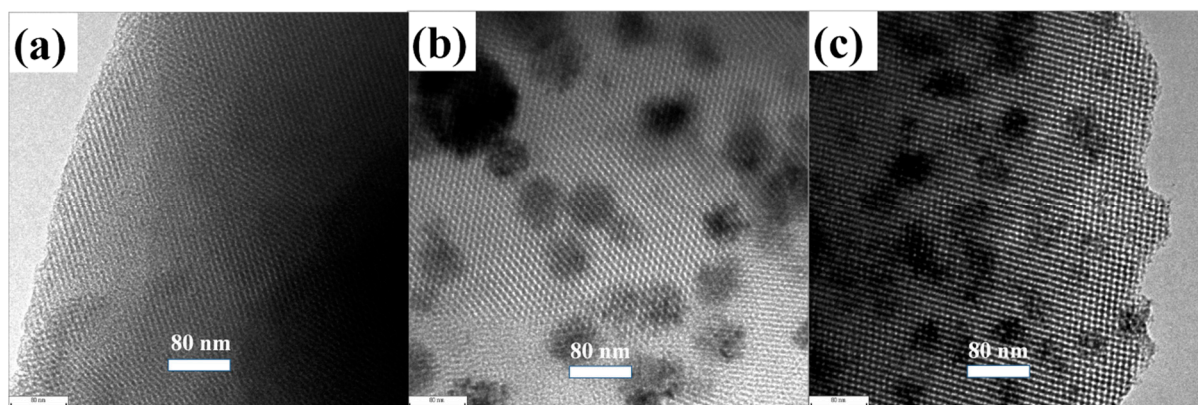


Figure 3. TEM images of (a) KIT-6, (b) fresh 10 wt% NiO/KIT-6 and (c) used 10 wt% NiO/KIT-6.

Methane combustion took place on NiO/KIT-6 catalysts. Throughout the reaction, CH_4 underwent complete oxidation to form CO_2 and H_2O . As indicated in Figure 4, the catalytic activity of KIT-6 could be enhanced significantly by adding NiO. In addition, the catalytic activity of the NiO/KIT-6 catalyst increases consistently when the NiO loading amount reaches 10 wt%, while 10 wt% NiO/KIT-6 samples show high activity. T10, T50 and T90 are only 386 °C, 456 °C and 507 °C, respectively, higher than others [32,33]. When the NiO loading amount reaches 15 wt%, the catalytic activity shows little change, because NiO nanoparticles destroy much of the the pore tunnel, resulting in the aggregation of NiO nanoparticles.

The textural properties and catalytic activities of all the samples are shown in Table 1. We estimated NiO particle size in the catalyst according to the diffraction peaks of cubic phase NiO using the Scherrer equation. The result shows that the particle size of NiO changes a little when the loading amounts increase, which is consistent with the wide diffraction peaks of NiO and means the NiO particles are dispersed well on KIT-6 without clumping. It is shown that there is only a tiny change in pore size, indicating that the pore structure is preserved even after using support NiO, which is in agreement with previous results. However, the BET surface areas and pore volume of NiO/KIT-6 samples decrease gradually with an increase in the NiO loading amount, due to the destruction of partial mesopores after NiO incorporation.

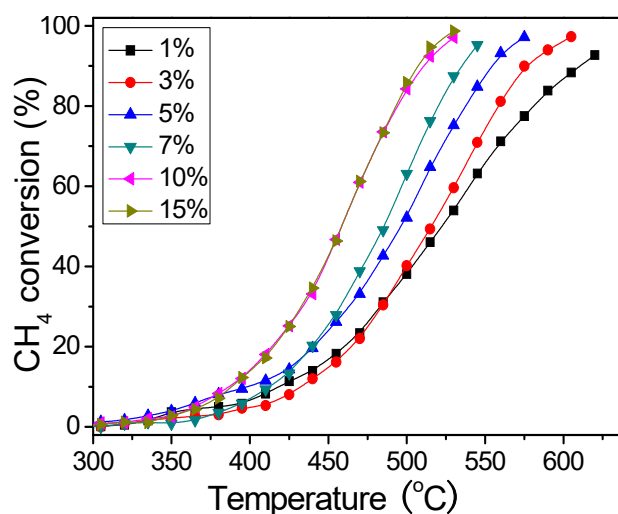


Figure 4. Light-off curves of catalytic combustion of methane using NiO/KIT-6 catalysts.

Table 1. Textural properties and catalytic activities of KIT-6 and KIT-6 support NiO samples.

| Samples | NiO Crystallite Size (nm) ^a | BET Surface Area (m ² ·g ⁻¹) | Average Pore Diameter (nm) | Pore Volume (cm ³ ·g ⁻¹) | Catalytic Activity in CH ₄ Combustion | | |
|---------------------------------------|--|---|----------------------------|---|--|----------------------|----------------------|
| | | | | | T ₁₀ (°C) | T ₅₀ (°C) | T ₉₀ (°C) |
| KIT-6 | – | 708 | 8.2 | 0.94 | – | – | – |
| 1 wt% NiO/ KIT-6 | 7.63 | 671 | 8.1 | 0.91 | 420 | 523 | 611 |
| 3 wt% NiO/ KIT-6 | 7.39 | 638 | 7.9 | 0.87 | 432 | 515 | 577 |
| 5 wt% NiO/ KIT-6 | 7.60 | 619 | 7.8 | 0.83 | 396 | 496 | 554 |
| 7 wt% NiO/ KIT-6 | 7.41 | 546 | 7.6 | 0.72 | 411 | 485 | 535 |
| 10 wt% NiO/ KIT-6 | 7.65 | 468 | 7.5 | 0.60 | 386 | 456 | 507 |
| 15 wt% NiO/ KIT-6 | 8.07 | 407 | 7.5 | 0.51 | 386 | 457 | 510 |
| 10 wt% NiO/ KIT-6 (used) ^b | 8.56 | 357 | 7.5 | 0.48 | – | – | – |

^a Crystallite sizes were calculated from the diffraction peaks of cubic phase NiO using the Scherrer equation.

^b 10 wt% NiO/ KIT-6 catalyst was collected after reaction.

Figure 5 shows the H₂-TPR profiles of different NiO/KIT-6 catalysts. Two hydrogen consumption peaks can be observed for all NiO/KIT-6 catalysts, named α_1 and α_2 . The α_1 peak, centered at ~355 °C, is attributed to the reduction of NiO species of low interaction with KIT-6 [34–36]. Additionally, the high temperature reduction peak (α_2 peak) is due to the reduction of NiO, which strongly interacted with KIT-6 to form a few surface layers made up of silicate-type compounds [34–36]. The area of the α_2 peak does not change obviously with the increase in the loading amount from 0.01 to 0.15, revealing that only a small number of NiO nanoparticles have strong interaction with the support. Therefore, the interaction between KIT-6 and NiO is weak, similar to the SBA-15 support catalyst [36], and the strong interaction is not a key factor for the improvement of activity.

To investigate the reason behind the high performance of NiO/KIT-6 catalysts, CH₄-TPSR was utilized and the findings are depicted in Figure 6. It is evident that without any oxygen introduced into the feed, methane oxidation can only occur through interaction with surface oxygen and bulk oxygen (at high temperatures) [37]. As shown in Figure 6, two CO₂ generation peaks can be observed over both samples, named β_1 and β_2 , which could correspond to the oxidation of methane by surface oxygen and bulk oxygen, respectively. The area of the β_1 peak for 10 wt% NiO/ KIT-6 is similar to that of pure NiO, but the NiO amount on NiO/ KIT-6 is only 10 percent that of the pure NiO sample. Therefore, the surface oxygen of NiO/ KIT-6 shows higher activity due to the high dispersion of NiO on KIT-6. Differing from pure NiO, the bulk oxygen of NiO/ KIT-6 can be reduced by CH₄ in a narrow temperature region.

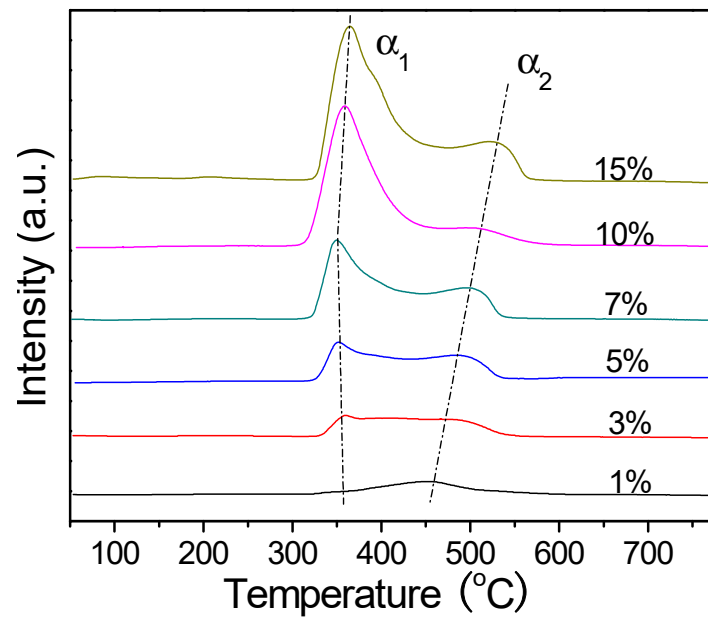


Figure 5. H₂-TPR profiles of KIT-6-supported NiO catalysts.

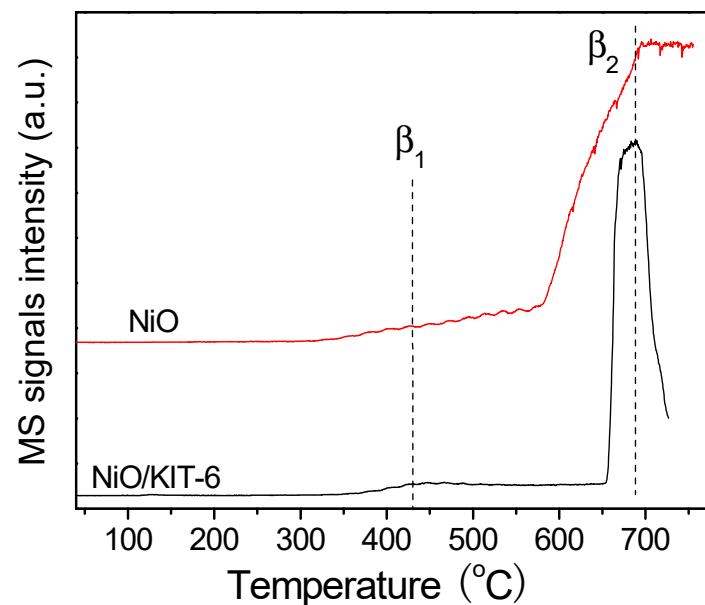


Figure 6. MS signals of CO₂ ($m/z = 44$) in the CH₄-TPSR of NiO and 10 wt% NiO/ KIT-6 catalysts.

The effect of the support is also investigated. The observed activities of the 10 wt% NiO/KIT-6, 10 wt% NiO/SBA-15, 10 wt% NiO/MCF and 10 wt% NiO/SiO₂ catalysts are shown in Figure 7. It was found that the catalytic activities of methane combustion with NiO-based catalysts decrease in the following order: NiO/KIT-6 > NiO/SBA-15 > NiO/MCF \approx NiO/SiO₂. The BET surface areas of KIT-6, SBA-15, MCF and SiO₂ are 708, 520, 562 and 387 m²·g⁻¹, respectively. Therefore, the remarkable enhancement in activity of NiO/KIT-6 compared to NiO/SBA-15 and NiO/SiO₂ can be attributed to its 3D pore connectivity, as well as its large surface area and pore volume [38]. Though MCF also has 3D mesopores, the large pore size of MCF (15/30 nm) cannot restrict the aggregation of NiO nanoparticles effectively when NiO nanoparticles are incorporated into the pore channels.

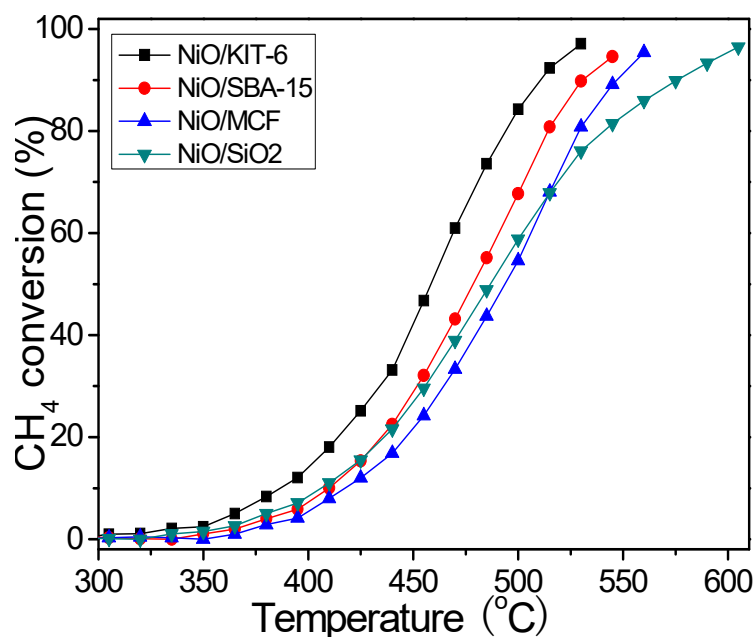


Figure 7. Methane combustion with 10 wt% NiO/KIT-6, 10 wt% NiO/SBA-15, 10 wt% NiO/MCF and 10 wt% NiO/SiO₂ catalysts.

After reaction, the used 10 wt% NiO/KIT-6 catalyst was collected for analysis. As shown in Figure 8a, the used catalyst has a sharp intense peak and a hump, as does the fresh catalyst, which reveals that the ordered mesoporous structure is retained even after reaction. Figure 8b shows that the wide-angle XRD patterns of the used catalyst are similar to those of the fresh one, without any growth of NiO particle size. There is a decrease in the surface area of the used catalyst, as it is exhibited in Table 1, due to the destruction of partial mesopores. Figure 3c shows the TEM image of the used catalyst. It can be seen clearly that the ordered mesopores remain and there is no obvious difference in pore size between the fresh catalyst and the used one. Additionally, the sizes of the NiO nanoparticles in the used catalyst are remarkably similar to those of the fresh one. The deactivation of nickel-based catalysts primarily occurs due to the formation of carbon deposits, which can take shape as carbon nanotubes during methane reforming, decomposition or partial oxidation [39–41]. However, no carbon nanotubes and carbon nanoparticles were observed in the TEM images, which reveals that there is no carbon deposit formation on the surface. The H₂-TPR results (not shown here) show that the reduction peaks (peak temperature and peak area) of the used catalyst are nearly the same as the fresh one, which means the used catalyst may still maintain a high reduction property.

FT-IR spectroscopy was used to investigate the surface group change of the used catalyst. As shown in Figure 9a, both samples have the characteristic band of the KIT-6 framework (bands at ~1085 and 799 cm⁻¹), corresponding to the T–O asymmetric stretching vibrations and T–O symmetric stretching vibrations, respectively [42]. The CO₃²⁻ group (bands at ~1350 and 1520 cm⁻¹), which can combine with Ni²⁺ ions to generate carbonates and then result in deactivation, was not observed in the FT-IR spectrum of the used catalyst. Therefore, there is no significant change to the NiO/KIT-6 catalyst during the combustion of methane. However, as displayed in Table 1, there is a decrease in the surface area of the catalyst, owing to the destruction of partial mesopores in the reaction. So, future work should focus on the enhancement of the thermal stability of the NiO/KIT-6 catalyst.

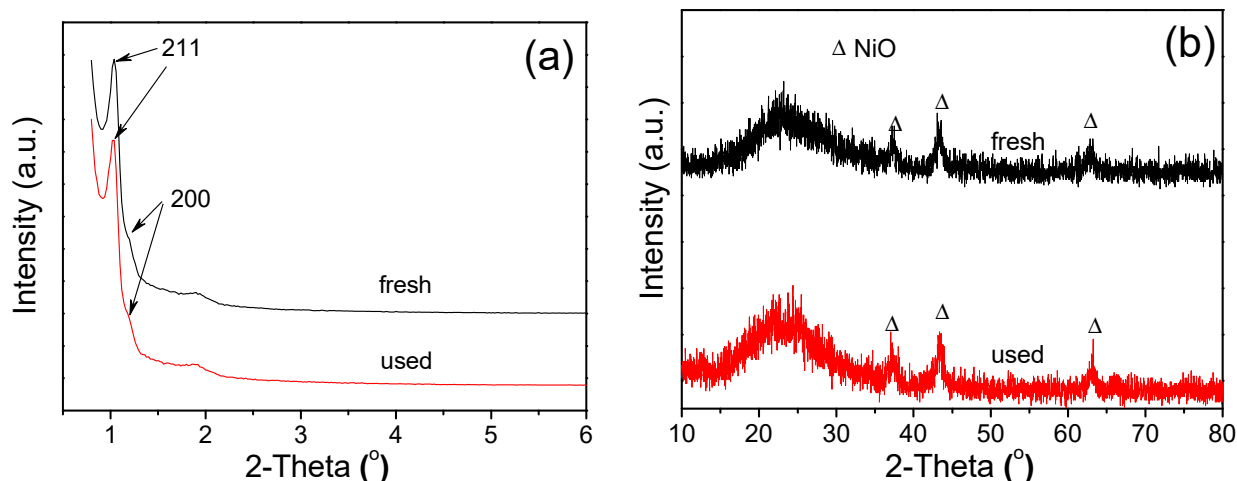


Figure 8. (a) Low-angle XRD patterns of fresh and used 10% NiO/KIT-6 catalyst; (b) wide-angle XRD patterns of fresh and used 10% NiO/KIT-6 catalyst (Δ NiO: NiO diffraction peak).

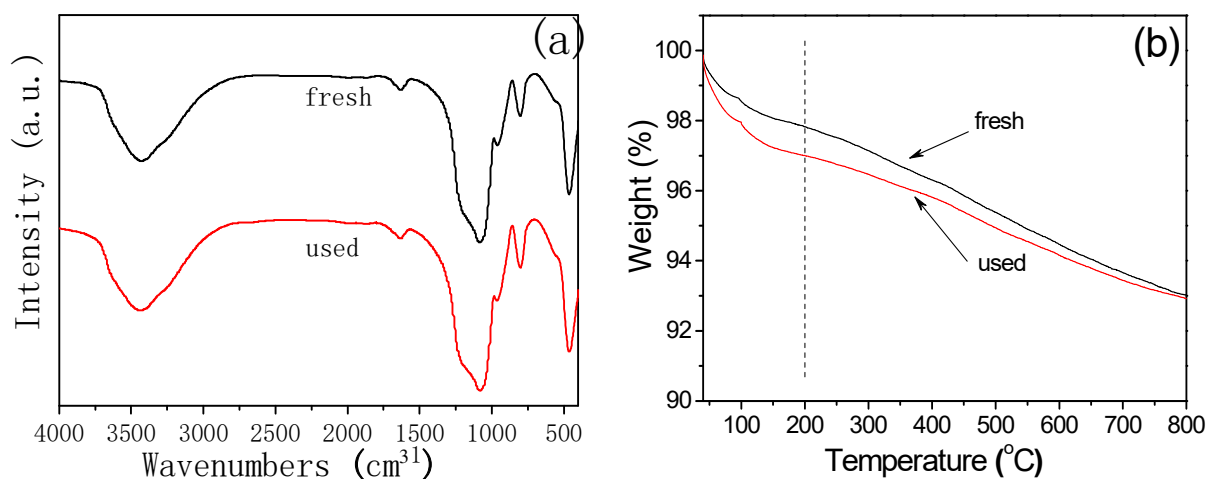


Figure 9. (a) FT-IR spectra of fresh and used 10 wt% NiO/KIT-6 catalysts and (b) TG curves of fresh and used 10% NiO/KIT-6 catalysts.

TG-DTA curves of the fresh and used 10% NiO/KIT-6 catalysts are presented in Figure 9b. It can be seen that, below 200 °C, the weight loss values of both samples are about 3%, attributed to removal of crystalline water, in agreement with the FT-IR spectra results. At above 200 °C, the tiny weight loss of the used catalyst is similar to the fresh one, which reveals that there is no carbon deposit formation on the surface, in agreement with the TEM results. Therefore, there is no obvious change in the NiO/KIT-6 catalyst during the combustion of methane.

4. Conclusions

In this paper, a series of NiO/KIT-6 catalysts were prepared for methane combustion, and the conclusions are as follows:

(1) The main well-ordered mesopore remains after NiO loading. However, some mesoporous structures are destroyed when a mass of NiO nanoparticles is incorporated.

(2) The characterization results show that the 10 wt% NiO/KIT-6 catalyst exhibits a high BET surface area and ordered 3D mesopores, and the NiO/KIT-6 catalyst has a high reduction property and catalytic performance in methane combustion, with T10, T50 and T90 being only 386 °C, 456 °C and 507 °C, respectively.

(3) NiO particle size changes a little as the loading amounts increase, and NiO particles are dispersed well on KIT-6. However, with the further increase in the load, the destruction of mesopores will lead to a decrease in the BET surface area and pore volume.

(4) Only a small amount NiO nanoparticles strongly interact with the support. Therefore, the interaction between KIT-6 and NiO is weak, so the strong interaction is not a key factor for the improvement of activity. Hence, the high performance of the NiO/KIT-6 catalyst may be due to the high dispersion of NiO and the good mass transfer property.

(5) There is no carbon deposit formation and no obvious difference in pore size between the fresh catalyst and the used one, and it still maintains a high activity.

In summary, the NiO/KIT-6 catalyst is an efficient methane combustion catalyst.

In future research, we will focus on the catalytic mechanism of CH₄ combustion over NiO/KIT-6, improve the activity and stability of the catalyst by doping Ce or other elements and surface modification, and conduct additional tests including EDX and long term stability tests and so on.

Author Contributions: X.H.: Formal analysis; Investigation; Methodology; Writing—review and editing; Writing—original draft; W.Y.: Investigation; Software; Writing—original draft; Writing—review and editing; Z.L.: Investigation; Writing—original draft; Writing—review and editing; Q.L. and Y.T.: Investigation; Software; Writing—review and editing; J.L.: Conceptualization; Data curation; Writing—original draft; Writing—review and editing. All authors have read and agreed to the published version of the manuscript.

Funding: This research was funded by National Natural Science Foundation of China [No.62003215], National Natural Science Foundation of China [No.61903251] and the Shanghai Pujiang Program [No. 22PJ047].

Data Availability Statement: The data presented in this study are available on request from the corresponding author.

Conflicts of Interest: The authors declare no conflict of interest.

References

1. Wang, A.; Austin, D.; Song, H. Investigations of thermochemical upgrading of biomass and its model compounds: Opportunities for methane utilization. *Fuel* **2019**, *246*, 443–453. [[CrossRef](#)]
2. Sun, L.; Wang, Y.; Guan, N.; Li, L. Methane activation and utilization: Current status and future challenges. *Energy Technol.* **2020**, *8*, 1900826. [[CrossRef](#)]
3. He, L.; Fan, Y.; Bellettre, J.; Yue, J.; Luo, L. A review on catalytic methane combustion at low temperatures: Catalysts, mechanisms, reaction conditions and reactor designs. *Renew. Sustain. Energy Rev.* **2020**, *119*, 109589. [[CrossRef](#)]
4. Neuberger, S.; Pennemann, H.; Shanmugam, V.; Zapf, R.; Kolb, G. Promoting effect of Rh on the activity and stability of Pt-based methane combustion catalyst in microreactors. *Catal. Commun.* **2021**, *149*, 106202. [[CrossRef](#)]
5. Al-Fatesh, A.; Singh, S.K.; Kanade, G.S.; Atia, H.; Fakeeha, A.H.; Ibrahim, A.A.; El-Toni, A.M.; Labhasetwar, N.K. Rh promoted and ZrO₂/Al₂O₃ supported Ni/Co based catalysts: High activity for CO₂ reforming, steam–CO₂ reforming and oxy–CO₂ reforming of CH₄. *Int. J. Hydrog. Energy* **2018**, *43*, 12069–12080. [[CrossRef](#)]
6. Yang, W.; Kim, M.-Y.; Polo-Garzon, F.; Gong, J.; Jiang, X.; Huang, Z.; Chi, M.; Yu, X.; Wang, X.; Guo, Y. CH₄ combustion over a commercial Pd/CeO₂-ZrO₂ three-way catalyst: Impact of thermal aging and sulfur exposure. *Chem. Eng. J.* **2023**, *451*, 138930. [[CrossRef](#)]
7. Rezaei Shadegan, H.; Maghsoodi, S.; Ghanavati, B.; Shahbazi Kootenaee, A.; Azimi, A. Catalytic combustion of methane over La₂BCoO₆ perovskites containing Ni, Cu and Fe: Impact of B-sites on oxygen species and catalytic activity. *React. Kinet. Mech. Catal.* **2020**, *131*, 737–752. [[CrossRef](#)]
8. Huang, F.; Tian, M.; Zhu, Y.; Wang, X.; Wang, A.; Li, L.; Lin, J.; Wang, J. Fe-substituted Ba-hexaaluminate with enhanced oxygen mobility for CO₂ capture by chemical looping combustion of methane. *J. Energy Chem.* **2019**, *29*, 50–57. [[CrossRef](#)]
9. Zhao, K.; Li, Z.; Bian, L. CO₂ methanation and co-methanation of CO and CO₂ over Mn-promoted Ni/Al₂O₃ catalysts. *Front. Chem. Sci. Eng.* **2016**, *10*, 273–280. [[CrossRef](#)]
10. Ding, Y.; Wang, S.; Zhang, L.; Chen, Z.; Wang, M.; Wang, S. A facile method to promote LaMnO₃ perovskite catalyst for combustion of methane. *Catal. Commun.* **2017**, *97*, 88–92. [[CrossRef](#)]
11. Fan, X.; Li, L.; Jing, F.; Li, J.; Chu, W. Effects of preparation methods on CoAlO_x/CeO₂ catalysts for methane catalytic combustion. *Fuel* **2018**, *225*, 588–595. [[CrossRef](#)]
12. Rizamarhaiza, M.; Sufizar, A.; Hamimah Abdul, R.; Mohd Azham, A.; Mas Fawzi Mohd, A.; Hariati, T. Producing the Methane Conversion by Steam Methane Reforming Over SiO₂-NiO Catalyst. *J. Adv. Res. Fluid Mech. Therm. Sci.* **2022**, *99*, 28–34. [[CrossRef](#)]

13. Huang, X.; Li, J.; Wang, J.; Li, Z.; Xu, J. Catalytic combustion of methane over a highly active and stable NiO/CeO₂ catalyst. *Front. Chem. Sci. Eng.* **2020**, *14*, 534–545. [[CrossRef](#)]
14. Chai, R.; Zhang, Z.; Chen, P.; Zhao, G.; Liu, Y.; Lu, Y. Ni-foam-structured NiO-MO_x-Al₂O₃ (M = Ce or Mg) nanocomposite catalyst for high throughput catalytic partial oxidation of methane to syngas. *Microporous Mesoporous Mater.* **2017**, *253*, 123–128. [[CrossRef](#)]
15. Al-Fatesh, A.S.; Ibrahim, A.A.; AlSharekh, A.M.; Alqahtani, F.S.; Kasim, S.O.; Fakeeha, A.H. Iron catalyst for decomposition of methane: Influence of Al/Si ratio support. *Egypt. J. Pet.* **2018**, *27*, 1221–1225. [[CrossRef](#)]
16. Lu, Y.; Jiang, S.; Wang, S.; Zhao, Y.; Ma, X. Effect of the addition of Ce and Zr over a flower-like NiO-MgO (111) solid solution for CO₂ reforming of methane. *J. CO₂ Util.* **2018**, *26*, 123–132. [[CrossRef](#)]
17. Al-Fatesh, A.S.; Fakeeha, A.H.; Ibrahim, A.A.; Khan, W.U.; Atia, H.; Eckelt, R.; Seshan, K.; Chowdhury, B. Decomposition of methane over alumina supported Fe and Ni-Fe bimetallic catalyst: Effect of preparation procedure and calcination temperature. *J. Saudi Chem. Soc.* **2018**, *22*, 239–247. [[CrossRef](#)]
18. Fakeeha, A.H.; Arafat, Y.; Ibrahim, A.A.; Shaikh, H.; Atia, H.; Abasaheed, A.E.; Armbruster, U.; Al-Fatesh, A.S. Highly Selective Syngas/H₂ Production via Partial Oxidation of CH₄ Using (Ni, Co and Ni-Co)/ZrO₂-Al₂O₃ Catalysts: Influence of Calcination Temperature. *Processes* **2019**, *7*, 141. [[CrossRef](#)]
19. Fakeeha, A.; Ibrahim, A.A.; Aljuraywi, H.; Alqahtani, Y.; Alkhodair, A.; Alswaidan, S.; Abasaheed, A.E.; Kasim, S.O.; Mahmud, S.; Al-Fatesh, A.S. Hydrogen Production by Partial Oxidation Reforming of Methane over Ni Catalysts Supported on High and Low Surface Area Alumina and Zirconia. *Processes* **2020**, *8*, 499. [[CrossRef](#)]
20. Bukhari, S.; Chin, C.; Setiabudi, H.; Vo, D.-V.N. Tailoring the properties and catalytic activities of Ni/SBA-15 via different TEOS/P123 mass ratios for CO₂ reforming of CH₄. *J. Environ. Chem. Eng.* **2017**, *5*, 3122–3128. [[CrossRef](#)]
21. Lv, Y.; Xin, Z.; Meng, X.; Tao, M.; Bian, Z. Ni based catalyst supported on KIT-6 silica for CO methanation: Confinement effect of three dimensional channel on NiO and Ni particles. *Microporous Mesoporous Mater.* **2018**, *262*, 89–97. [[CrossRef](#)]
22. Tao, M.; Meng, X.; Lv, Y.; Bian, Z.; Xin, Z. Effect of impregnation solvent on Ni dispersion and catalytic properties of Ni/SBA-15 for CO methanation reaction. *Fuel* **2016**, *165*, 289–297. [[CrossRef](#)]
23. Pudukudy, M.; Yaakob, Z.; Akmal, Z.S. Direct decomposition of methane over SBA-15 supported Ni, Co and Fe based bimetallic catalysts. *Appl. Surf. Sci.* **2015**, *330*, 418–430. [[CrossRef](#)]
24. Murthy, P.R.; Zhang, J.-C.; Li, W.-Z. Exceptionally stable sol-immobilization derived Pd/SBA-15 catalysts for methane combustion. *Catal. Sci. Technol.* **2021**, *11*, 3609–3618. [[CrossRef](#)]
25. MERKACHE, R. 3D ordered mesoporous Fe-KIT-6 catalysts for methylcyclopentane (MCP). In Proceedings of the International Conference on Materials Science ICMS2018, Sétif, Algeria, 12–14 September 2018.
26. Tang, C.; Huang, J.; Zhang, D.; Jiang, Q.; Zhou, G. CO₂ utilization by dry reforming of CH₄ over mesoporous Ni/KIT-6 catalyst. *Int. J. Chem. React. Eng.* **2021**, *19*, 1167–1178. [[CrossRef](#)]
27. Mahfouz, R.; Estephane, J.; Gennequin, C.; Tidahy, L.; Aouad, S.; Abi-Aad, E. CO₂ reforming of methane over Ni and/or Ru catalysts supported on mesoporous KIT-6: Effect of promotion with Ce. *J. Environ. Chem. Eng.* **2021**, *9*, 104662. [[CrossRef](#)]
28. Kleitz, F.; Choi, S.H.; Ryoo, R. Cubic Ia3d large mesoporous silica: Synthesis and replication to platinum nanowires, carbon nanorods and carbon nanotubes. *Chem. Commun.* **2003**, *9*, 2136–2137. [[CrossRef](#)] [[PubMed](#)]
29. Zhao, D.; Feng, J.; Huo, Q.; Melosh, N.; Fredrickson, G.H.; Chmelka, B.F.; Stucky, G.D. Triblock copolymer syntheses of mesoporous silica with periodic 50 to 300 angstrom pores. *Science* **1998**, *279*, 548–552. [[CrossRef](#)]
30. Schmidt-Winkel, P.; Lukens, W.W.; Yang, P.; Margolese, D.I.; Lettow, J.S.; Ying, J.Y.; Stucky, G.D. Microemulsion Templating of Siliceous Mesoporous Cellular Foams with Well-Defined Ultralarge Mesopores. *Chem. Mater.* **2000**, *12*, 686–696. [[CrossRef](#)]
31. Miao, Y.; Lu, G.; Liu, X.; Guo, Y.; Wang, Y.; Guo, Y. Effects of preparation procedure in sol-gel method on performance of MoO₃/SiO₂ catalyst for liquid phase epoxidation of propylene with cumene hydroperoxide. *J. Mol. Catal. A Chem.* **2009**, *306*, 17–22. [[CrossRef](#)]
32. Li, Y.; Guo, Y.; Xue, B. Catalytic combustion of methane over M (Ni, Co, Cu) supported on ceria-magnesia. *Fuel Process. Technol.* **2009**, *90*, 652–656. [[CrossRef](#)]
33. Thaicharoensutcharittham, S.; Meeyoo, V.; Kitiyanan, B.; Rangsunvigit, P.; Rirksomboon, T. Catalytic combustion of methane over NiO/Ce_{0.75}Zr_{0.25}O₂ catalyst. *Catal. Commun.* **2009**, *10*, 673–677. [[CrossRef](#)]
34. Zapata, B.; Valenzuela, M.A.; Palacios, J.; Torres-Garcia, E. Effect of Ca, Ce or K oxide addition on the activity of Ni/SiO₂ catalysts for the methane decomposition reaction. *Int. J. Hydrog. Energy* **2010**, *35*, 12091–12097. [[CrossRef](#)]
35. Nakamura, N.; Takahashi, R.; Sato, S.; Sodesawa, T.; Yoshida, S. Ni/SiO₂ catalyst with hierarchical pore structure prepared by phase separation in sol-gel process. *Phys. Chem. Chem. Phys.* **2000**, *2*, 4983–4990. [[CrossRef](#)]
36. Pompeo, F.; Nichio, N.N.; González, M.G.; Montes, M. Characterization of Ni/SiO₂ and Ni/Li-SiO₂ catalysts for methane dry reforming. *Catal. Today* **2005**, *107–108*, 856–862. [[CrossRef](#)]
37. Zenbourny, L.; Azambre, B.; Weber, J.V. Transient TPSR, DRIFTS-MS and TGA studies of a Pd/ceria-zirconia catalyst in CH₄ and NO₂ atmospheres. *Catal. Today* **2008**, *137*, 167–173. [[CrossRef](#)]
38. Takahashi, R.; Sato, S.; Tomiyama, S.; Ohashi, T.; Nakamura, N. Pore structure control in Ni/SiO₂ catalysts with both macropores and mesopores. *Microporous Mesoporous Mater.* **2007**, *98*, 107–114. [[CrossRef](#)]

39. Guevara, J.C.; Wang, J.A.; Chen, L.F.; Valenzuela, M.A.; Salas, P.; García-Ruiz, A.; Toledo, J.A.; Cortes-Jácome, M.A.; Angeles-Chavez, C.; Novaro, O. Ni/Ce-MCM-41 mesostructured catalysts for simultaneous production of hydrogen and nanocarbon methane decomposition. *Int. J. Hydrog. Energy* **2010**, *35*, 3509–3521. [[CrossRef](#)]
40. Takenaka, S.; Kobayashi, S.; Ogihara, H.; Otsuka, K. Ni/SiO₂ catalyst effective for methane decomposition into hydrogen and carbon nanofiber. *J. Catal.* **2003**, *217*, 79–87.
41. Zhu, J.; Peng, X.; Yao, L.; Shen, J.; Tong, D.; Hu, C. The promoting effect of La, Mg, Co and Zn on the activity and stability of Ni/SiO₂ catalyst for CO₂ reforming of methane. *Int. J. Hydrog. Energy* **2011**, *36*, 7094–7104. [[CrossRef](#)]
42. Soni, K.; Rana, B.S.; Sinha, A.K.; Bhaumik, A.; Nandi, M.; Kumar, M.; Dhar, G.M. 3-D ordered mesoporous KIT-6 support for effective hydrodesulfurization catalysts. *Appl. Catal. B Environ.* **2009**, *90*, 55–63. [[CrossRef](#)]

Disclaimer/Publisher’s Note: The statements, opinions and data contained in all publications are solely those of the individual author(s) and contributor(s) and not of MDPI and/or the editor(s). MDPI and/or the editor(s) disclaim responsibility for any injury to people or property resulting from any ideas, methods, instructions or products referred to in the content.